ORGANOMETALLICS

pubs.acs.org/Organometallics

Article

Well-Stabilized but Strained Frustrated Lewis Pairs Based on Rh/N and Ir/N Couples

Carlos Ferrer, Joaquina Ferrer,* Vincenzo Passarelli, Fernando J. Lahoz, Pilar García-Orduña, and Daniel Carmona*

Cite This: *Organometallics* 2022, 41, 1445−1453

Read Online

ACCESS | Metrics & More | Article Recommendations | Supporting Information

ABSTRACT: The dimers $[(Cp^*MCl)_2(\mu\text{-}Cl)_2]$ ($Cp^* = \eta^5\text{-}C_5Me_5$) react with *N*-pyridin-2-ylmethyl-*N*′,*N*″-bis-(2,6-diisopropylphenyl)guanidine ($\mathbf{H_2L}$) in the presence of $NaSbF_6$, giving rise to chlorido compounds of formula $[Cp^*MCl(\kappa^2N,N'\text{-}\mathbf{H_2L})][SbF_6]$ (M = Rh, **1**; Ir, **2**), in which the guanidine ligand adopts a κ^2N,N' chelate coordination mode. Compounds **1** and **2** react with NaOH, rendering the complexes $[Cp^*M(\kappa^3N,N',N''\text{-}\mathbf{HL})][SbF_6]$ (M = Rh, **3**; Ir, **4**), in which the **HL** ligand exhibits a *fac* κ^3N,N',N'' coordination. Complexes **3** and **4** activate the H−H and O−H bonds of dihydrogen and water. The hydrido complex $[Cp^*IrH(\kappa^2N,N'\text{-}\mathbf{H_2L})][SbF_6]$ (**6**) was isolated from the reaction of the iridium complex **4** with H_2. In the reaction of the rhodium complex **3** with D_2O, its Cp* ligand is gradually and reversibly deuterated. A plausible mechanism for this H/D exchange is proposed. The new complexes have been characterized by analytical and spectroscopic means, including the determination of the crystal structures of the compounds **1**−**4** and **6** by X-ray diffractometric methods.

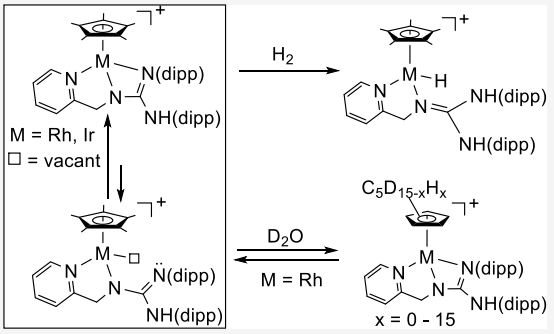

INTRODUCTION

The discovery by Stephan's group that species based on representative elements containing donor and acceptor sites, unable to form a Lewis adduct, cooperatively activate dihydrogen was a milestone in main-group-elements chemistry.[1] The term frustrated Lewis pair (FLP) was coined for this class of species.[2] Subsequently, it was demonstrated that FLPs are capable of activating a large variety of substrates, such as imines, olefins, alkynes, organic carbonyl compounds, carbon dioxide, and so on[3−5] and catalyzing several organic reactions.[6−10] Notably, Wass's group showed that it is possible to incorporate transition-metal components into FLPs, which gave rise to the so-called transition metal frustrated Lewis pairs (TMFLPs).[11] The interest in the latter is rooted in the fact that they are able to combine transition metal and FLP reactivity in a synergistic fashion.[12−14] In this respect, it has to be noted that TMFLP reactivity constitutes a particular case of metal−ligand cooperative reactivity.[15]

An interesting peculiarity of the FLP species is that, even when the acidic and basic components annihilate each other as a consequence of the formation of the corresponding Lewis adduct, they can still exhibit FLP reactivity as long as the dissociation is thermally viable. Indeed, provided that the dissociated form is thermally accessible, the formation of the Lewis adduct is not a drawback and turns out to be advantageous because it allows for the stabilization of the FLP species, which facilitates its storage and handling.[16] The terms "masked"[17] and "dormant"[18] have been used to refer to this type of FLPs.

During the last years, our research group has focused on the preparation and study of the reactivity of TMFLPs based on half-sandwich compounds bearing $(\eta^5\text{-}C_5Me_5)Rh(III)$[19] or $(\eta^6\text{-}p\text{-cymene})M(II)$ (M = Ru, Os) fragments.[20,21] A common and pivotal feature of these TMFLPs is that the included metal centers complete their coordination sphere, thanks to a monoanionic phosphano- or pyridinyl-guanidine ligand exhibiting a *fac* κ^3 coordination (Scheme 1A), thus ensuring the stabilization of the resulting complex. Concomitantly, the complex features fused five- and four-membered metalacycles and the central nitrogen atom adopts a pyramidal sp^3 hybridization. A close inspection of the molecular structure of these complexes[19−21] revealed that the structural parameters within the four-membered M−N−C−N metalacycle deviate significantly from those expected for an ideal hybridization of its atoms, therefore suggesting that this ring undergoes a high strain. Consequently, the metalacycle is prone to relieve this strain by means of the cleavage of the metal-iminic nitrogen bond under mild conditions, providing a vacant site at the

Received: April 8, 2022
Published: June 1, 2022

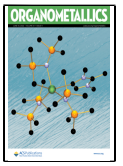

Scheme 1. (A) Phosphano- and Pyridinyl-guanidino TMFLPs; (B) New Pyridinyl-guanidine Ligand

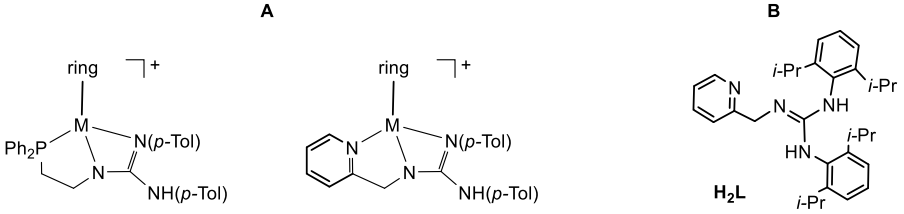

Scheme 2. Synthesis of the Ligand H_2L and of the Chlorido Complexes 1 and 2

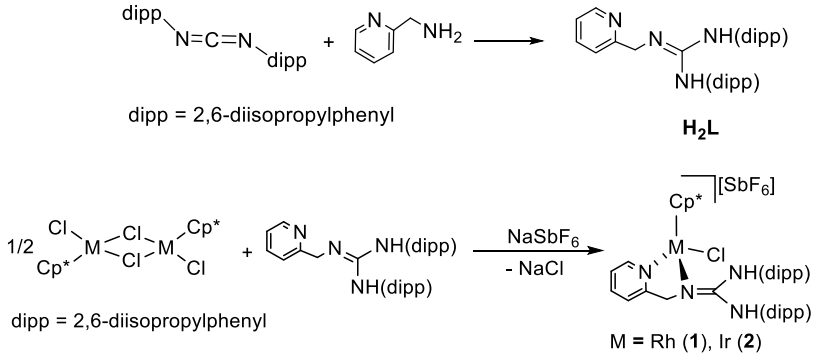

metal and a lone electron pair on the involved nitrogen, that is, these compounds are masked TMFLPs.

The study of the reactivity of these phosphano- and pyridinyl-guanidino complexes, bearing *para*-tolyl (*p*-Tol) substituents in the guanidine moiety, has sometimes been hindered by the metalation of the *ortho* carbon of the *p*-Tol group. Actually, this side reaction masks the processes under study and can even prevent them. To overcome these drawbacks, we have now designed and prepared the new pyridinyl-guanidine ligand $\mathbf{H_2L}$ depicted in Scheme 1B. As a matter of fact, the new ligand gathers all the features that we have just pointed out as necessary to generate TMFLPs and, additionally, the presence of isopropyl substituents in the 2 and 6 positions of the arene groups prevents metalation reactions.

Herein, we report on the preparation and characterization of the masked rhodium and iridium TMFLP compounds $[Cp^*M(\kappa^3N,N',N''\text{-}\mathbf{HL})][SbF_6]$ and the reactivity of these complexes with H_2 and H_2O. We also report on an unusual and reversible hydrogen abstraction from the Cp* methyl groups that results in gradual and complete H/D exchange when deuterated water is employed.

RESULTS AND DISCUSSION

Synthesis of the Chlorido Complexes $[Cp^*MCl(\kappa^2N,N'\text{-}H_2L)][SbF_6]$. The ligand $\mathbf{H_2L}$ has been prepared by reacting 1,3-bis(2,6-diisopropylphenyl) carbodiimide with-2-(aminomethyl)pyridine in THF (Scheme 2) following literature procedures.[22]

Reaction of the dimers $[(Cp^*MCl)_2(\mu\text{-}Cl)_2]$[23] with the pyridinyl-guanidine compound $\mathbf{H_2L}$ in the presence of $NaSbF_6$ affords the chlorido complexes $[Cp^*MCl(\kappa^2N,N'\text{-}\mathbf{H_2L})][SbF_6]$ (M = Rh, **1**; Ir, **2**; Scheme 2).

The complexes were characterized by analytical and spectroscopic means (see the Experimental Section). Assignment of the NMR signals was verified by two-dimensional homonuclear and heteronuclear correlations. Remarkably, the methylene protons of the pyridinyl-guanidine ligand are asynchronous, giving an AB system. This feature suggests a κ^2N,N' coordination mode of the ligand which would render stereogenic the metal center and diastereotopic the methylene protons of the nitrogenated ligand. Weak IR bands in the 2950−3350 cm^{-1} region together with ^1H NMR singlets at 7.82 and 5.77 ppm (complex **1**) and at 7.58 and 5.80 ppm (complex **2**) are indicative of the presence of two NH groups in the molecule.

Synthesis of the Complexes $[Cp^*M(\kappa^3N,N',N''\text{-}HL)][SbF_6]$. Treatment of the chloride derivatives **1** and **2** with NaOH affords the complexes $[Cp^*M(\kappa^3N,N',N''\text{-}\mathbf{HL})][SbF_6]$ (M = Rh, **3**; Ir, **4**), in which the **HL** ligand adopts a κ^3N,N',N'' coordination mode. Formally, the reaction consists of the elimination of HCl from the starting complexes by treatment with a base (Scheme 3).

Scheme 3. Synthesis of the Complexes 3 and 4

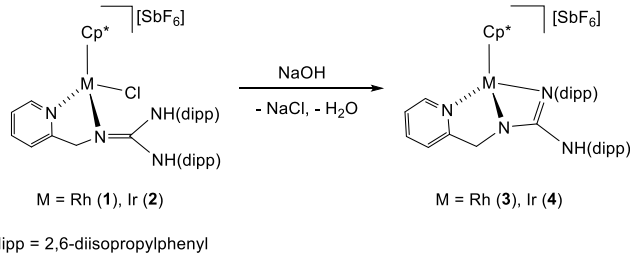

An IR band at 2967 and 3379 cm^{-1} for complexes **3** and **4**, respectively, and a broad ^1H singlet at 6.35 and 6.58 ppm for **3** and **4**, respectively, are attributed to the remaining NH functionality. As a consequence of the stereogenicity of the metal, the methylene protons are asynchronous. ^1H signals centered at 4.08 and 3.37 ppm and at 3.95 and 3.55 ppm are attributed to these protons in the rhodium and iridium complexes, respectively.

Molecular Structure of the Complexes $[Cp^*MCl(\kappa^2N,N'\text{-}H_2L)][SbF_6]$ and $[Cp^*M(\kappa^3N,N',N''\text{-}HL)][SbF_6]$. To unequivocally establish the solid state structure of the new complexes, their crystal structure was determined by X-ray

https://doi.org/10.1021/acs.organomet.2c00172
Organometallics 2022, 41, 1445−1453

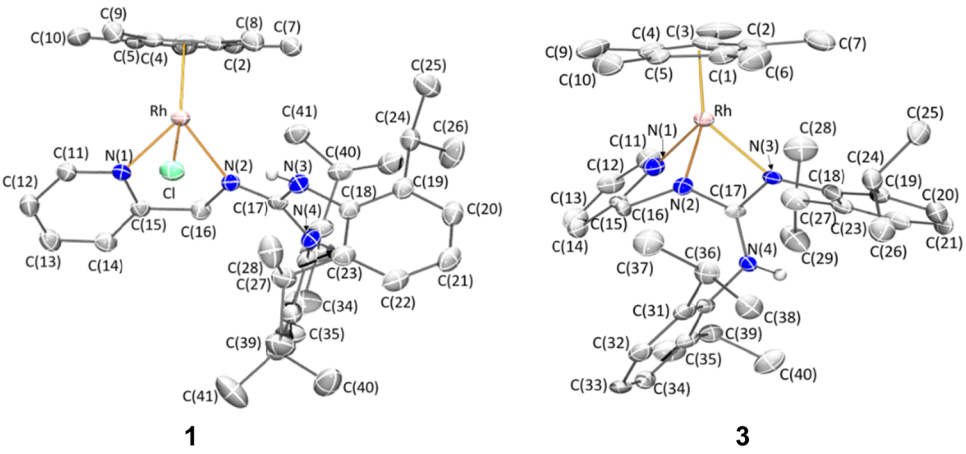

Figure 1. Molecular structure of the cation of complexes **1** and **3**. For clarity, all the hydrogen atoms are omitted, except the N−H protons.

diffraction analysis. In all four compounds, the metal is a stereogenic center. Complexes **1** and **2** crystallize in the tetragonal $I4_1/a$ space group and complex **3** in the orthorhombic $Pna2_1$ space group. Therefore, in all three cases, the two chiral-at-metal enantiomers are present in the unit cell. However, the iridium complex **4** crystallizes in the chiral monoclinic $P2_1$ space group, and therefore, each of the two enantiomers crystallizes separately.

Comparable structural parameters are found for the cation of complexes **1** and **2** as well as for that of **3** and **4**. Hence, only the structural parameters found in the rhodium compounds **1** and **3** will be discussed here. For the most relevant structural parameters of the iridium complexes **2** and **4**, see Supporting Information. A view of the molecular structure of the cation of **1** and **3** is depicted in Figure 1, and relevant characteristics of their metal coordination spheres are summarized in Table 1. In both cases, the cation exhibits the so-called "three-legged piano-stool" geometry with a Cp* group occupying three *fac* positions. In the cation of **1**, the guanidine ligand $\mathbf{H_2L}$ displays a κ^2N,N' chelating coordination and a chlorine atom completes the coordination sphere of the metal. In complex **3**, the three remaining coordination sites are occupied by the deprotonated guanidine ligand **HL** adopting a *fac* κ^3N,N',N'' coordination mode. According to the ligand priority sequence,[24−26] Cp* > Cl > N(2) > N(1) in complex **1** and Cp* > N(3) > N(1) > N(2) in complex **3**, the configuration of the enantiomer depicted in Figure 1 is S_{Rh} for both cations.

Table 1. Selected Bond Lengths (Å) and Angles (°) for Complexes 1 and 3

	1	3
Rh-Ct[a]	1.7882(2)	1.7788(2)
Rh-Cl	2.4015(6)	
Rh-N(3)		2.133(6)
Rh-N(1)	2.092(2)	2.153(6)
Rh-N(2)	2.1435(19)	2.090(6)
Ct[a]-Rh-Cl	122.34(1)	
Ct[a]-Rh-N(3)		135.69(1)
Ct[a]-Rh-N(1)	130.66(1)	128.92(92)
Ct[a]-Rh-N(2)	133.38(1)	134.28(1)
N(1)-Rh-Cl	87.27(6)	
N(1)-Rh-N(3)		92.2(2)
N(2)-Rh-Cl	90.55(5)	
N(2)-Rh-N(3)		62.5(2)
N(1)-Rh-N(2)	77.16(7)	76.5(2)
C(17)-N(2)	1.312(3)	1.364(9)
C(17)-N(3)	1.374(3)	1.294(9)
C(17)-N(4)	1.368(3)	1.361(9)

[a]Ct stands for the centroid of the Cp* ligand

The structural parameters associated with the guanidine CN_3 core deserve some comments (Scheme 4). Going from complex **1** to **3**, the geometry at the central nitrogen atom N(2) of the pyridinyl-guanidine ligand switches from planar (Σ°N(2) = 359.2 (3)° in **1**) to pyramidal (Σ°N(2) = 322.1 (8)° in **3**), suggesting that the change from the κ^2N,N' coordination of $\mathbf{H_2L}$ in **1** to the *fac* κ^3N,N',N'' coordination of **HL** in **3** entails a change of the hybridization of N(2) from sp^2 to sp^3. Moreover, the metal-bonded terminal nitrogen atom N(3) in **3** features a planar geometry (Σ°N(3) = 359.4 (9)°), suggesting that a sp^2 hybridization should correspond to this nitrogen atom. On the other hand, as far as the carbon−nitrogen bond lengths are concerned, the shortest bond length of the chlorido **1** is observed for the central nitrogen atom N(2), C(17)−N(2) 1.312 (3) Å, whereas the metal-bonded terminal nitrogen atom N(3) exhibits the shortest carbon−nitrogen bond length in **3**, C(17)−N(3) 1.294 (9) Å. Taking into account that the sum of the double bond covalent radii of carbon and nitrogen is 1.27 Å,[27] a certain degree of delocalization among the three C−N bonds in each complex (Table 1) may be concluded. Nonetheless, when **1** converts into **3**, the deprotonation/coordination of $\mathbf{H_2L}$ clearly brings about an electronic redistribution within the CN_3 core, which formally shifts the carbon−nitrogen double bond from the C(17)−N(2) bond of **1** to the C(17)−N(3) bond of **3** (Scheme 4). Overall, the versatility of the stereo-electronic properties of the pyridinyl-guanidine ligand facilitates, when deprotonated, the coordination of the terminal nitrogen atom N(3) to the metal, with the concomitant formation of the four-membered metalacycle Rh−N(2)−C(17)−N(3). Despite the formation of this metalacycle, a strong strain within it is inferred from the small N(2)−Rh−N(3) and N(2)−C(17)−N(3) angles, 62.5 (2)° and 111.1 (6)°, respectively, far from the ideal values. Consequently, the cleavage of the Rh−N(3) bond of **3**, which generates active basic and acidic FLP sites in the cation, would be triggered by this strain. Thus, we envisioned that the rhodium complex **3** could be considered a masked TMFLP, as it will be shown in the next section.

https://doi.org/10.1021/acs.organomet.2c00172
Organometallics 2022, 41, 1445−1453

Scheme 4. Structural Details of the Pyridinyl-guanidine Ligand in Complexes 1 and 3

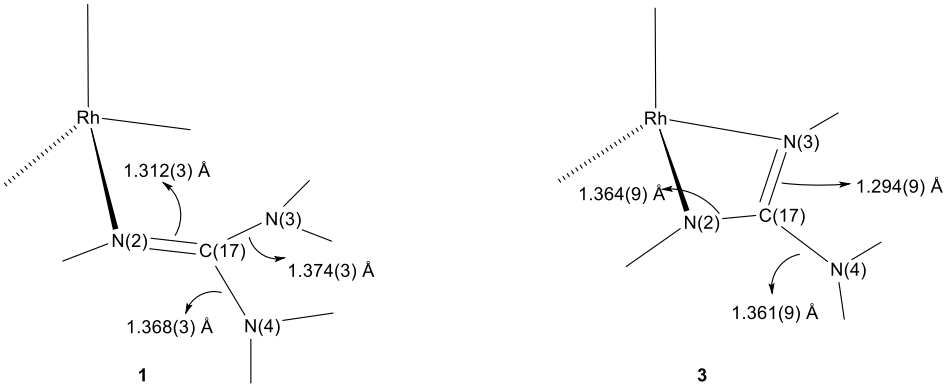

Reaction of the Complexes 3 and 4 with H_2. Showing a typical FLP reactivity,[14] complexes **3** and **4** heterolytically activate molecular hydrogen, affording metal-hydrido complexes of formula $[Cp^*MH(\kappa^2N,N'\text{-}\mathbf{H_2L})][SbF_6]$ (M = Rh, **5**; Ir, **6**), in which a new N−H functionality has formed (Scheme 5).

Scheme 5. Reaction of Complexes 3 and with Molecular Hydrogen

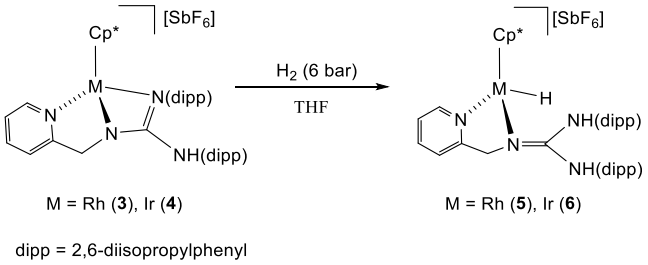

To achieve acceptable reaction rates, the iridium complex **4** has to be treated with H_2 (6 bar) at temperatures higher than 323 K. However, above 373 K, decomposition of the complex was apparent. An optimal temperature of 353 K was established. At this temperature, quantitative conversion of complex **4** was achieved after 120 h of treatment with H_2 at an initial pressure of 6 bar. Under these conditions, about 8% of ligand dissociation was observed and pure complex **6** was isolated in 62% yield.

At 298 K, under 6 bar of H_2, the ^{1}H NMR spectrum of THF solutions of the rhodium complex **3** shows the formation of the hydrido complex **5** (δH = −8.22 ppm, ^1J(RhH) = 26.9 Hz). The reaction rate is very slow; after 48 h of treatment, under these conditions, only about 5% of conversion to the hydrido complex **5** was determined by ^{1}H NMR spectroscopy. The concomitant appearance of small amounts of free pyridinyl-guanidine ligand was observed. At higher reaction temperatures, the conversion to hydride **5** increases, but the dissociation of the pyridinyl-guanidine ligand increases even more, thus preventing the isolation of pure **5** in acceptable yields.

The molecular structure of complex **6** was determined by X-ray diffraction. The complex crystallizes as a racemate in the orthorhombic $Pna2_1$ space group. An ORTEP view of the cation of **6** is depicted in Figure 2, and a selection of its bond lengths and angles is collected in the caption of Figure 2. The coordination sphere of the metal consists of an η^5-Cp* group

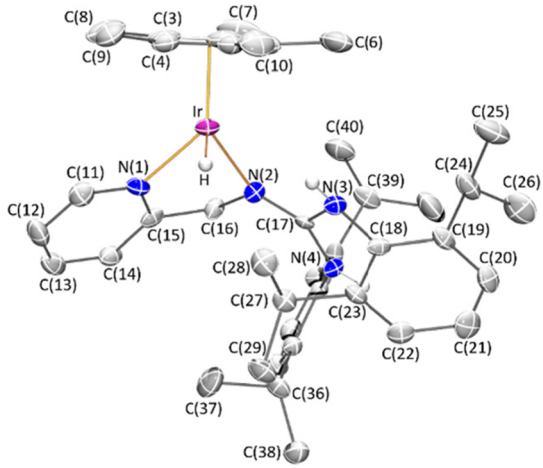

Figure 2. Molecular structure of the cation of complex **6**. For clarity, all the hydrogen atoms are omitted, except hydride and the N-H protons. Selected bond lengths (Å) and angles (°) are as follows: Ir−Ct 1.8288 (1), Ir−N(1) 2.082 (6), Ir−N(2) 2.101 (6), Ir−H 1.60, N(2)−C(17) 1.311 (9), N(3)−C(17) 1.379 (8), N(3)−C(18) 1.440 (9), N(4)−C(17) 1.367 (9), Ct−Ir−N(1) 130.47 (1), Ct−Ir−N(2) 132.65 (1), Ct−Ir−H 118, N(1)−Ir−N(2) 76.4 (2), N(1)−Ir−H 86.6, N(2)−Ir−H 99.0, C(17)−N(3)−C(18) 122.0 (6), C(17)−N(3)−H(3 N) 114 (6), C(18)−N(3)−H(3 N) 114 (6); Ct, centroid of the Cp* ligand.

occupying three *fac* positions, the guanidine ligand $\mathbf{H_2L}$ displaying a κ^2N,N' chelating coordination mode, and a hydrogen atom. According to the ligand priority sequence,[24−26] Cp* > N(2) > N(1) > H, the configuration of the enantiomer depicted in Figure 2 is S_{Ir}. The structural parameters within the guanidine core CN_3 [(Σ°N(2) = 358.5 (9)°, C(17)−N(2) = 1.311 (9) Å, C(17)−N(3) = 1.379 (8) Å, C(17)−N(4) = 1.367 (9) Å] closely resemble those measured for the chlorido complexes **1** (Table 1, Scheme 4) and **2** (Supporting Information), in which the pyridinyl-guanidine ligand adopts a κ^2N,N' chelating coordination mode. Therefore, again, a change in the coordination mode (in this case, from the *fac* κ^3N,N',N'' of **HL** in **3** to the κ^2N,N' coordination of $\mathbf{H_2L}$ in **6**) implies a change of the hybridization of coordinated N(2) atom (from sp^3 to sp^2).

Reaction of the Complexes 3 and 4 with D_2O. No significant changes in the ^{1}H NMR spectrum of THF-d_8 solutions of the rhodium complex **3** were observed when excess H_2O was added. However, when at 333 K, a THF-d_8/D_2O (78%/22%, v/v) solution of the complex was monitored

https://doi.org/10.1021/acs.organomet.2c00172
Organometallics 2022, 41, 1445−1453

by ^{1}H NMR, a gradual decrease of the singlet attributed to the Cp* protons along with the concomitant appearance of a broad signal at almost the same chemical shift was observed (Figure 3).

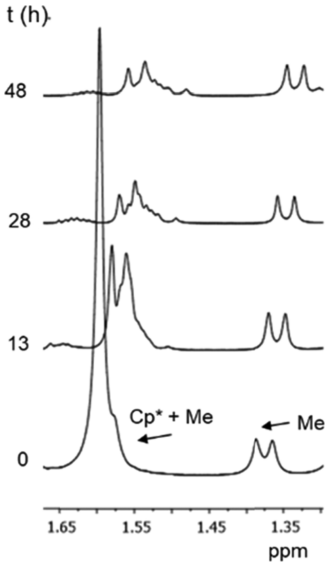

Figure 3. Monitoring of the sequential deuteration of complex **3** by NMR. Evolution of the ^{1}H NMR spectra of complex **3** in 78% THF-d_8/22% D_2O at 333 K.

The rest of the proton spectrum remains essentially unchanged. Figure 4 shows the concurrent variation over time of the mass spectra of the solution. These data can be accounted for by assuming the progressive deuteration of the methyl groups of the Cp* ligand up to the **3**-d^{15} isotopologue.

Although it is generally accepted that the Cp* is a non-reactive ligand, a few cases have been described in which the inter- or intramolecular hydrogen abstraction from the methyls of this ligand by a strong base results in H/D exchange processes.[19,28−30] On the basis of the DFT calculations carried out on the related phosphano-guanidinato complex of rhodium [Cp*Rh(κ^3*P,N′,N″*-**HL**)][SbF_6],[19] a plausible mechanism would involve (Scheme 6): (i) activation of a D_2O molecule to afford the deuteroxy intermediate **I**; (ii) proton abstraction from the Cp* methyl by the coordinated OD group in **I** providing the tetramethylfulvene complex **II**, in which a formal reduction from Rh(III) to Rh(I) has taken place; and (iii) a fast coordinated-HDO/D_2O-solvent exchange on **II**. The reversibility of the step **I** ⇄ **II** and **3** ⇄ **I** would result in the progressive deuteration of the Cp* ligand.

It is remarkable that the stereo-electronic rearrangement within the CN_3 core that we have discussed for the conversion of **1** into **3** (see Scheme 4) takes place in the opposite direction in the **3** ⇄ **I** sequence. All in all, the important role that the guanidine ligand plays in the reactivity of the FLP species is revealed.

As its rhodium analogue, the iridium complex **4** also undergoes H/D exchange of its Cp* hydrogen in D_2O solutions but at a much slower rate. In fact, a maximum corresponding to the **4**-d^2 isotopologue was observed in the mass spectrum of a sample of complex **4** in THF-d_8/D_2O (78%/22%, v/v) solution heated at 383 K for 72 h.

CONCLUSIONS

A judicious design of the ligand allows for the synthesis of η^5-pentamethyl cyclopentadienyl half-sandwich complexes of rhodium(III) and iridium(III), which behave as masked TMFLPs. As a key feature, the ligand has to be able to coordinate with the metal in a *fac* κ^3 fashion. In this way, it formally occupies the coordination hemisphere left free by the Cp* ligand, completes the external electronic configuration of the metal up to 18 electrons, and stabilizes the resulting metal complex. In order for the ligand to acquire the required *fac* coordination mode, the central nitrogen atom of the ligand has to adopt an sp^3 hybridization. No less important is the fact that the arrangement of the coordinating atoms must be able to give rise to a strained metalacycle, namely, a four-membered cycle in the compounds described herein. The strain release associated with the opening of this metalacycle favors the thermal access to the active FLP form.

The pyridinyl-guanidine compound **H_2L** depicted in Scheme 1B, once deprotonated, fulfills all these prerequisites.

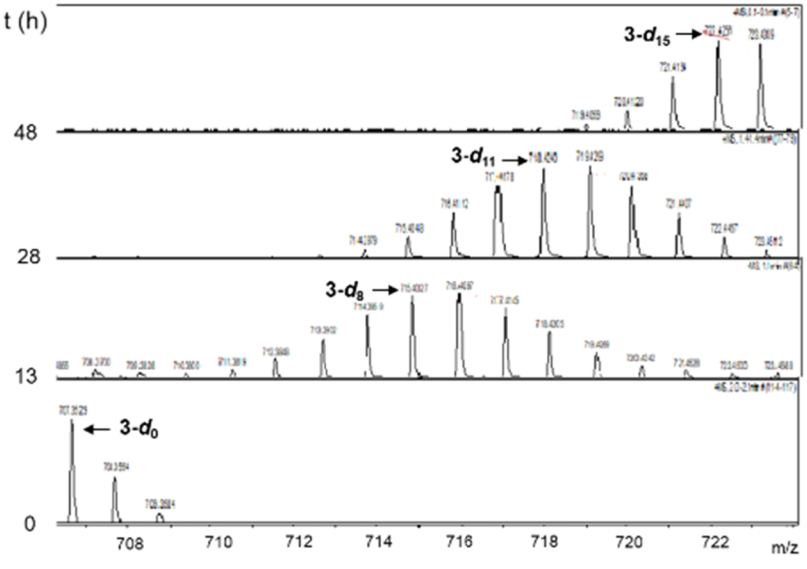

Figure 4. Monitoring of the sequential deuteration of complex **3** by MS. Evolution of the mass spectra of **3** in 78% THF-d_8/22% D_2O at 333 K.

https://doi.org/10.1021/acs.organomet.2c00172
Organometallics 2022, 41, 1445−1453

Scheme 6. Proposed Mechanism for the H/D Exchange Process

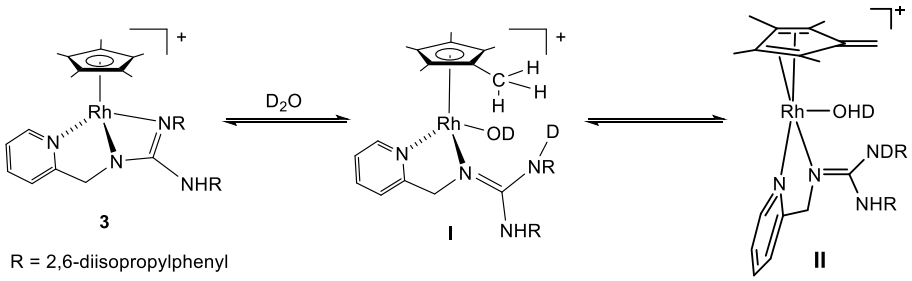

Furthermore, the ability of the CN_3 guanidine core to undergo an electronic redistribution within the three C−N bonds plays an important role fulfilling the electronic requirements of the diverse geometries adopted by the ligand (see Scheme 4). It is also worth mentioning the protecting role of the isopropyl groups in positions 2 and 6 of the aryl substituents of the guanidine nitrogen atoms. Under mild conditions, aryls without substituents in these positions undergo cyclometalation reactions that mask or preclude the desired FLP reactivity of the complexes.

The derived complexes $[Cp^*M(\kappa^3N,N',N''\text{-}\mathbf{HL})][SbF_6]$ (M = Rh, **3**; Ir, **4**) behave as masked FLPs. Strain-releasing M−N bond cleavage makes accessible FLP sites and, following FLP reactivity patterns, they activate the H−H and the water O−H bonds. When D_2O was employed, activation of the $C(sp^3)$−H bonds of the Cp* methyl groups results in an unusual and reversible H/D exchange. On the basis of DFT calculations carried out on related half-sandwich complexes, the plausible intervention of a Rh−OD intermediate may be invoked.

In summary, the studies reported in this article pave the way for extending the synthesis of masked TMFLPs to other tridentate ligands as well as other metal ions. We believe that with the wide variety of stereo-electronic properties that can be achieved in the new TMFLP species, new processes for both small molecule activation and catalysis can be successfully addressed. Efforts in the framework of this line of research are currently underway in our laboratory.

EXPERIMENTAL SECTION

General Information. All solvents were treated in a PS-400-6 Innovative Technologies Solvent Purification System (SPS). Infrared spectra were recorded on a Perkin-Elmer Spectrum-100 (ATR mode) FT-IR spectrometer. Carbon, hydrogen, and nitrogen analyses were performed using a Perkin-Elmer 240 B microanalyzer. ^1H and ^{13}C spectra were recorded on Bruker AV-300 (300.13 MHz) or Bruker AV-400 (400.16 MHz) spectrometers. Chemical shifts are expressed in ppm up field from $SiMe_4$; J values are given in Hz. COSY, NOESY, HSQC, HMQC, and HMBC ^1H-X (X = ^1H, ^{13}C) correlation spectra were obtained using standard procedures. Mass spectra were obtained with a Micro Tof-Q Bruker Daltonics spectrometer.

Preparation of the Complexes $[Cp^*MCl(\kappa^2N,N'\text{-}H_2L)][SbF_6]$ (M = Rh (1), Ir (2)). Under an argon atmosphere, to a suspension of the corresponding dimer $[(Cp^*MCl)_2(\mu\text{-}Cl)_2]$ (0.480 mmol) in methanol (8 mL), a solution of $\mathbf{H_2L}$ (457 mg, 0.970 mmol) in the same solvent (2 mL) and $NaSbF_6$ (251 mg, 0.970 mmol) were added. The precipitation of a solid took place (Rh), and the resulting suspension or solution (Ir) was stirred overnight. The solvent was evaporated to dryness, and the orange (Rh) or yellow (Ir) residue was extracted with dichloromethane (3 × 5 mL). The resulting solution was concentrated under reduced pressure to ca. 0.3 mL. Slow addition of *n*-pentane led to the precipitation of a solid. The supernatant liquid was decanted with a cannule, and the solid was washed with *n*-pentane (3 × 10 mL) and vacuum-dried. Yield: 675 mg, 71% (Rh); 910 mg, 89% (Ir). Crystals suitable for X-ray diffraction analysis were obtained by crystallization from CH_2Cl_2/MeOH/Et_2O/*n*-pentane solutions of **1** or **2**.

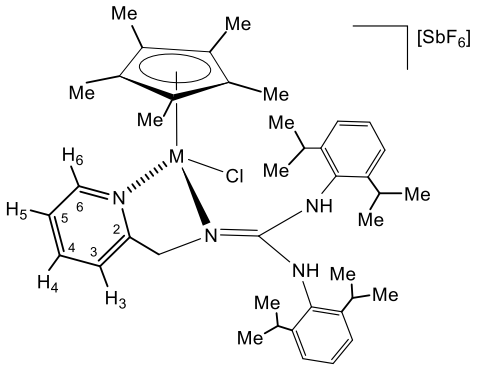

M = Rh (**1**), Ir (**2**)

Complex **1**. Anal. calcd for $C_{41}H_{57}ClF_6N_4RhSb$: C, 50.25; H, 5.86; N, 5.72. Found: C, 49.90; H, 5.67; N, 5.69. HRMS (μ-TOF): $C_{41}H_{57}ClN_4Rh$ $[M\text{-}SbF_6]^+$: calcd 743.3321, found 743.3317. IR (cm^{-1}): ν(NH) 3335 (w), 2966 (w); ν(C═N), Py) 1602 (s); ν(C═N) 1570 (s); $\nu(SbF_6)$ 654 (s).

^1H NMR (400.16 MHz, CD_2Cl_2, 298 K, ppm): δ = 8.44 (d, J = 5.4 Hz, 1H, H_6), 7.82 (bs, 1H, NH *cis* to Rh), 7.81 (td, J = 7.7, 1.5 Hz, 1H, H_4), 7.48 (m, 1H, H_5), 7.43 (d, J = 8.0 Hz, 1H, Ar), 7.39 (d, J = 7.5 Hz, 1H, Ar), 7.32 (m, 3H, Ar), 7.19 (dd, J = 7.7, 1.5 Hz, 1H, Ar), 6.79 (d, J = 7.9 Hz, 1H, H_3), 5.77 (s, 1H, NH *trans* to Rh), 4.31, 4.15 (AB system, J = 17.0 Hz, 2H, CH_2), 3.53, 3.42, 3.20, 2.73 (4 × m, 4H, CH(*i*Pr)), 1.71 (s, 15H, C_5Me_5), 1.55, 1.42 (2 × d, J = 6.9, 6.9 Hz, 6H, Me_2(*i*Pr)), 1.31, 1.19 (2 × d, J = 6.7, 6.8 Hz, 6H, Me_2(*i*Pr)), 1.24, 1.16 (2 × d, J = 6.8, 6.6 Hz, 6H, Me_2(*i*Pr)), 0.94, 0.81 (2 × d, J = 6.9, 6.8 Hz, 6H, Me_2(*i*Pr)). *$^{13}C\{^1H\}$ NMR (100.62 MHz, CD_2Cl_2, 298 K, ppm)*: δ = 161.9 (C_2), 155.4 (C═N), 151.9 (C_6), 149.2, 148.6, 146.1 (4 × C(*i*Pr)), 139.8 (C_4), 132.5, 130.4, 130.3, 130.2 (4 × C_{Ar}), 126.1 (C_5), 125.7, 125.2, 125.0, 124.9 (4 × C_{Ar}), 121.1 (C_3), 96.4 (d, J_{RhC} = 8 Hz, C_5Me_5), 58.6 (CH_2), 29.1, 28.9, 28.8, 28.6 (4 × CH(*i*Pr)), 28.6, 27.4, 26.4, 24.0, 23.6, 23.5, 23.0, 22.4 (8 × Me(*i*Pr)), 9.5 (C_5Me_5).

Complex **2**. Anal. calcd for $C_{41}H_{57}IrClF_6N_4Sb$: C, 46.05; H, 5.37; N, 5.24. Found: C, 46.16; H, 5.59; N, 5.14. HRMS (μ-TOF): $C_{41}H_{57}IrClN_4$ $[M\text{-}SbF_6]^+$: calcd 833.3901, found 833.3887. IR (cm^{-1}): ν(NH) 3348 (w), 3234 (w); ν(C═N) 1606 (s), $\nu(SbF_6)$ 650 (s). *^1H NMR (400.16 MHz, CD_2Cl_2, 298 K, ppm)*: δ = 8.42 (d, J = 5.1 Hz, 1H, H_6), 7.81 (td, J = 7.8, 1.5 Hz, 1H, H_4), 7.58 (s, 1H, NH *cis* to Ir), 7.49−7.37 (m, 3H, H_5, Ar), 7.37−7.27 (bm, 3H, Ar), 7.20 (dd, J = 7.7, 1.5 Hz, 1H, Ar), 6.87 (d, J = 7.9 Hz, 1H, H_3), 5.80 (s, 1H, NH *trans* to Ir), 4.58, 4.04 (AB system, J = 16.8 Hz, 2H, CH_2), 3.49, 3.39, 3.29, 2.75 (4 × m, 4H, CH(*i*Pr)), 1.70 (s, 15H, C_5Me_5), 1.51, 1.42 (2 × d, J = 6.9, 6.9 Hz, 6H, Me_2(*i*Pr)); 1.29, 1.26 (2 × d, J = 6.8, 6.9 Hz, 6H, Me_2(*i*Pr)); 1.19, 1.15 (2 × d, J = 6.8, 6.5 Hz, 6H, Me_2(*i*Pr)), 0.94, 0.82 (2 × d, J = 6.9, 6.8 Hz, 6H, Me_2(*i*Pr)). *$^{13}C\{^1H\}$ NMR (75.48 MHz, CD_2Cl_2, 298 K, ppm)*: δ = 162.2 (C_2), 155.1 (C═N), 151.7 (C_6), 149.5, 146.3, 146.2 (4 × C(*i*Pr)), 140.2 (C_4), 132.4, 130.6, 130.5, 130.1 (4 × C_{Ar}), 126.5 (C_5), 125.9, 125.4, 125.2 (4 × C_{Ar}), 120.8 (C_3), 88.4 (C_5Me_5), 60.0 (CH_2), 29.1, 29.0, 28.8, 28.7 (4

https://doi.org/10.1021/acs.organomet.2c00172
Organometallics 2022, 41, 1445−1453

× CH(*i*Pr)), 27.5, 26.4, 24.1, 23.8, 23.7, 23.2, 22.4 (8 × Me(*i*Pr)), 9.5 (C_5Me_5).

Preparation of the Complexes [Cp*M((κ^3*N,N′,N″*-HL)][SbF_6] (M = Rh (3), Ir (4)). At 278 K, to a solution of the corresponding complex [Cp*MCl(κ^2*N,N′*-**H_2L**)][SbF_6] (0.20 mmol) in 9:1 (v/v) THF/toluene (10 mL), a solution of NaOH (12 mg, 0.30 mmol) in H_2O (2 mL) was added. The biphasic suspension was stirred for 30 min, and then 10 mL of H_2O was added. The organic phase was extracted with a 9:1 (v/v) solution of THF/toluene (3 × 10 mL) and evaporated to dryness. The obtained orange (Rh) or yellow (Ir) residue was washed with toluene (3 × 5 mL) and vacuum-dried. Recrystallization from CH_2Cl_2/diethyl ether/*n*-pentane afforded complexes **3** and **4**. Yield: 136 mg, 71% (Rh); 141 mg, 68% (Ir). Crystals suitable for X-ray diffraction analysis were obtained by crystallization from CH_2Cl_2/diethyl ether/*n*-pentane solutions of **3** or **4**.

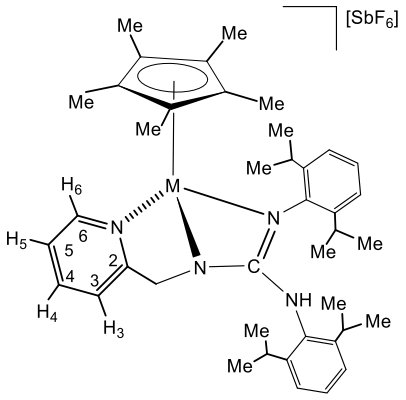

M = Rh (**3**), Ir (**4**)

Complex ***3***. Anal. calcd for $C_{41}H_{56}F_6N_4RhSb$: C, 52.19; H, 5.98; N, 5.94. Found: C, 51.74; H, 6.06; N, 6.08. HRMS (*μ*-TOF): $C_{41}H_{56}N_4Rh$ [M-SbF_6]$^+$: calcd 707.3555, found 707.3529. IR (cm^{-1}): *ν*(NH) 2967 (w); *ν*(C═N), Py) 1593 (s); *ν*(C═N) 1557 (s); *ν*(SbF_6) 654 (s). ^{1}*H NMR (400.16 MHz, THF-d*$_8$*, 298 K, ppm)*: *δ* = 9.03 (d, *J* = 5.4 Hz, 1H, H_6), 7.92 (td, *J* = 7.7, 1.4 Hz, 1H, H_4), 7.71 (t, *J* = 6.4 Hz, 1H, H_5), 7.43 (d, *J* = 8.0 Hz, 1H, Ar), 7.39 (d, *J* = 7.5 Hz, 1H, Ar), 7.32 (m, 3H, Ar), 7.19 (dd, *J* = 7.7, 1.5 Hz, 1H, Ar), 6.79 (d, *J* = 7.9 Hz, 1H, H_3), 6.35 (bs, 1H, NH), 4.08, 3.37 (AB system, *J* = 18.1 Hz, 2H, CH_2), 3.49, 3.06, 2.44, 2.16 (4 × m, 4H, CH(*i*Pr)), 1.64 (s, 15H, C_5Me_5), 1.64 (bs, overlapped, 3H, Me(*i*Pr)), 1.44 (d, *J* = 6.7 Hz, 3H, Me(*i*Pr)), 1.33 (d, *J* = 6.5 Hz, 3H, Me(*i*Pr)), 1.23 (d, *J* = 6.7 Hz, 3H, Me(*i*Pr)), 1.31, 0.70 (2 × d, *J* = 6.1, 6.7 Hz, 6H, Me_2(*i*Pr)), 0.78, 0.77 (2 × d, *J* = 6.7, 6.7 Hz, 6H, Me_2(*i*Pr)). $^{13}C\{^1H\}$ *NMR (100.62 MHz, THF-d*$_8$*, 298 K, ppm)*: *δ* = 169.4 (C_2), 167.6 (C═N), 152.4 (C_6), 147.1, 146.5, 145.2, 144.6 (4 × C*i*Pr), 140.0 (C_4), 131.4, 129.5, 125.9, 124.3, 123.4 (5 × C_{Ar}), 123.2 (C_5), 122.4, 122.0, 121.9 (3 × C_{Ar}), 120.2 (C_3), 94.5 (d, J_{RhC} = 8 Hz, C_5Me_5)), 56.7 (CH_2), 29.6, 28.8, 28.7, 28.3 (4 × CH(*i*Pr)), 26.9, 26.8, 25.9, 24.5, 24.2, 23.9, 23.9, 23.6 (8 × Me(*i*Pr)), 9.0 (C_5Me_5).

Complex ***4***. Anal. calcd for $C_{41}H_{56}F_6IrN_4Sb$: C, 47.68; H, 5.46; N, 5.42. Found: C, 47.62; H, 5.42; N, 5.55. HRMS (*μ*-TOF): $C_{41}H_{56}IrN_4$ [M-SbF_6]$^+$: calcd 797.4134, found 797.4146. IR (cm^{-1}): *ν*(NH) 3379 (w); *ν*(C═N) 1555 (s); *ν*(SbF_6) 655 (s). ^{1}*H NMR (400.16 MHz, THF-d*$_8$*, 298 K, ppm)*: *δ* = 9.05 (d, *J* = 5.4 Hz, 1H, H_6), 7.94 (t, *J* = 7.5 Hz, 1H, H_4), 7.68 (t, *J* = 6.3 Hz, 1H, H_5), 7.43−7.03 (bm, 7H, 6Ar, H_3), 6.58 (bs, 1H, NH), 3.95, 3.55 (AB system, *J* = 18.1 Hz, 2H, CH_2), 3.46, 3.38, 3.10, 2.56 (4 × m, 4H, CH(*i*Pr)), 1.63 (s, 15H, Me (C_5Me_5)), 1.63 (bs, overlapped, 3H, Me(*i*Pr)), 1.46 (d, *J* = 6.6 Hz, 3H, Me(*i*Pr)), 1.31 (pt, *J* = 6.3 Hz, 6H, 2 × Me(*i*Pr)); 1.23, 0.87 (2 × d, *J* = 6.6, 6.7 Hz, 6H, Me_2(*i*Pr)), 0.80, 0.73 (2 × d, *J* = 6.8, 6.8 Hz, 6H, Me_2(*i*Pr)). $^{13}C\{^1H\}$ *NMR (100.62 MHz, THF-d*$_8$*, 298 K, ppm)*: *δ* = 172.9 (C_2), 169.8 (C═N), 152.4 (C_6), 146.7, 146.5, 146.0, 144.9 (4 × C*i*Pr); 139.9 (C_4), 133.5, 131.7, 128.9, 127.7, 126.4 (5 × C_{Ar}), 126.4 (C_5); 125.2, 124.9, 123.4 (3 × C_{Ar}), 120.2 (C_3), 86.7 (C_5Me_5)), 56.6 (CH_2), 29.7, 28.8, 28.7, 28.4 (4 × CH (*i*Pr)), 27.0, 25.9, 24.5, 24.1, 24.0, 23.5, 23.9, 23.6 (8 × Me (*i*Pr)), 9.1 (C_5Me_5).

Preparation of [Cp*IrH(κ^2*N,N′-*H_2**L)][SbF_6] (6).** H_2 gas (6 bar) was added to a high-pressure NMR tube containing a solution of the complex [Cp*Ir(κ^3*N,N′,N″-***HL***)][SbF_6] (50 mg, 0.048 mmol) in THF-d_8 (0.45 mL). The resulting solution was monitorized by proton NMR. A mixture of complex **6** (80%)-uncoordinated ligand **H_2L** (about 8%) and small amounts of two unidentified hydrido complexes, which do not contain pyridinyl-guanidine ligand, was observed after 120 h of reaction at 353 K. The solvent was evaporated to dryness, and the residue was washed with diethyl ether (3 × 5 mL). Pure complex **6** was obtained by recrystallization from acetone/diethyl ether/*n*-pentane. Yield: 31 mg, 62%.

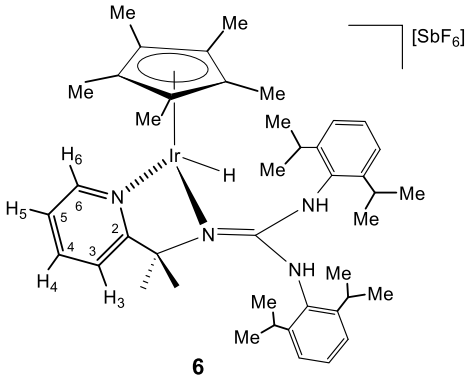

6

Complex ***6***. Anal. calcd for $C_{41}H_{58}IrF_6N_4Sb{\cdot}2H_2O$: C, 45.98; H, 5.84; N, 5.23. Found: C, 45.98; H, 6.08; N, 5.18. HRMS (*μ*-TOF): $C_{41}H_{58}IrN_4$ [M-SbF_6]$^+$: calcd 799.4291, found 799.4315. IR (cm^{-1}): *ν*(NH) 3357 (w), 3281 (w); *ν*(Ir-H) 2059 (s); *ν*(C═N) 1623 (br); *ν*(SbF_6) 656 (s). ^{1}*H NMR (300.13 MHz, THF-d*$_8$*, 298 K, ppm)*: *δ* = 8.61 (d, *J* = 5.4 Hz, 1H, H_6), 7.77 (t, *J* = 7.4 Hz, 1H, H_4), 7.51−7.26 (m, 6H, Ar, H_5), 7.19 (d, J = 7.6, 1H, Ar), 7.07 (s, 1H, NH *cis* to Ir), 6.86 (d, *J* = 7.6 Hz, 1H, H_3), 6.57 (s, 1H, NH *trans* to Ir), 4.46, 4.09 (AB system, *J* = 16.7 Hz, 2H, CH_2), 3.65−3.31 (m, 2H, CH(*i*Pr)), 3.09, 2.70 (2 × m, 4H, CH(*i*Pr)), 1.85 (d, *J* = 0.56 Hz, 15H, C_5Me_5), 1.51, 1.42 (2 × d, *J* = 6.8, 6.8 Hz, 6H, Me_2(*i*Pr)); 1.34−1.19 (4 × m, 12H, Me_2(*i*Pr); 0.91, 0.63 (2 × d, *J* = 6.8, 6.8 Hz, 6H, Me_2(*i*Pr)), −9.61(s, 1H, Ir-H). $^{13}C\{^1H\}$ *NMR (75.48 MHz, THF-d*$_8$*, 298 K, ppm)*: *δ* = 163.8 (C_2), 154.5 (C═N), 154.3 (C_6), 149.8, 149.0, 147.6 (4 × C(*i*Pr)), 139.6 (C_4), 134.4, 132.2, 130.8, 130.7, 126.1, 126.0, 125.6, 125.3, 125.1 (8 × C_{Ar}, C_5), 121.4 (C_3), 89.6 (C_5Me_5), 60.8 (CH_2), 30.1, 29.6, 29.4, 29.4 (4 × CH(*i*Pr)), 27.5, 26.8, 25.4, 24.1, 23.8, 23.8, 23.6, 22.1 (8 × Me(*i*Pr)), 10.3 (C_5Me_5).

X-Ray Crystallography. X-ray diffraction data were collected on a Smart APEX (compound **2**), APEX DUO (complexes **1** and **3**), and D8 VENTURE (complex **4** and **6**) Bruker diffractometers, using graphite-monochromated Mo *κα* radiation (*λ* = 0.71073 Å). Single crystals were mounted on a fiber or a MiTeGen support, coated with a protecting perfluoropolyether oil, and cooled to 100 (2) K with an open-flow of nitrogen gas. Data were collected using *ω*-scans (and *φ* scans in complex **4** and **6** data collection) with narrow oscillation frame strategies. Diffracted intensities were integrated and corrected of absorption effects by using a multi-scan method using SAINT[31] and SADABS[32,33] programs, included in APEX2 or APEX4 packages. Structures were solved by direct methods with SHELXS[34] and refined by full-matrix least squares on F^2 with the SHELXL program[35] included in the Wingx program system.[36]

Hydrogen atoms have been observed in Fourier difference maps. Most of them have been included in the model in calculated positions and refined with a riding model. Those of NH fragments have been included in observed positions, with geometrical restraints concerning N−H bond lengths.

Large solvent accessible voids are observed in the unit cell of complexes **1** and **2**. However, the solvent is highly disordered, and no attempt to include it in the model leads to adequate results. Therefore, Squeeze corrections[37] have been applied. The total

https://doi.org/10.1021/acs.organomet.2c00172
Organometallics 2022, 41, 1445−1453

potential accessible void volume and the electron count agree with the presence of 16 and 24 diethyl ether molecules in the unit cell for **1** and **2**, respectively. They have been taken into account in the chemical formula, F000 and density.

Structural Data for ***1***. $C_{41}H_{57}ClF_6N_4RhSb\cdot C_4H_{10}O$; M_r = 1054.13; red prism, 0.260 × 0.260 × 0.360 mm^3; tetragonal $I4_1/a$; a = 30.098 (3) Å, b = 30.098 (3) Å, c = 21.2679(19) Å; V = 19,266 (2) Å^3, Z = 16, D_c = 1.454 g/cm^3; μ = 1.019 cm^{-1}; min. and max. absorption correction factors: 0.6075 and 0.7246; $2\theta_{max}$ = 56.71°; 98,658 reflections measured, 11,999 unique; R_{int} = 0.0611; number of data/restraint/parameters 11,999/1/508; R_1 = 0.0312 [8957 reflections, $I > 2\sigma(I)$], $wR(F^2)$ = 0.0741 (all data); largest difference peak 1.017 e Å^{-3}.

Structural Data for ***2***. $C_{47}H_{57}ClF_6IrN_4Sb\cdot 1.5(C_4H_{10}O)$; M_r = 1175.95; yellow needle, 0.225 × 0.300 × 0.400 mm^3; tetragonal $I4_1/a$; a = 30.0816 (14) Å, b = 30.0816 (14) Å, c = 21.2997 (10) Å; V = 19,274 (2) Å^3, Z = 16, D_c = 1.621 g/cm^3; μ = 3.438 cm^{-1}; min. and max. absorption correction factors: 0.3425 and 0.4733; $2\theta_{max}$ = 58.094°; 113,852 reflections measured, 12,364 unique; R_{int} = 0.0284; number of data/restraint/parameters 12,364/1/508; R_1 = 0.0288 [11,436 reflections, $I > 2\sigma(I)$], $wR(F^2)$ = 0.0726 (all data); largest difference peak 1.732 e Å^{-3}.

Structural Data for ***3***. $C_{41}H_{56}F_6N_4RhSb$; M_r = 943.55; orange prism, 0.060 × 0.070 × 0.400 mm^3; orthorhombic $Pna2_1$; a = 29.893 (3) Å, b = 10.5046 (9) Å, c = 13.2394 (12) Å; V = 4157.3 (6) Å^3, Z = 4, D_c = 1.508 g/cm^3; μ = 1.107 cm^{-1}; min. and max. absorption correction factors: 0.7482 and 0.8633; $2\theta_{max}$ = 52.286°; 36,132 reflections measured, 8467 unique; R_{int} = 0.0454; number of data/restraint/parameters 8467/2/495; R_1 = 0.0398 [7542 reflections, $I > 2\sigma(I)$], $wR(F^2)$ = 0.0899 (all data); largest difference peak 1.437 e Å^{-3}, Flack parameter: −0.005 (11).

Structural Data for ***4***. $C_{41}H_{56}F_6IrN_4Sb$; M_r = 1032.84; yellow block, 0.105 × 0.130 × 0.130 mm^3; monoclinic $P2_1$; a = 10.8613 (4) Å, b = 13.1928 (5) Å, c = 14.4253 (6) Å, β = 97.5470 (10)°; V = 2049.11 (14) Å^3, Z = 2, D_c = 1.674 g/cm^3; μ = 3.964 cm^{-1}; min. and max. absorption correction factors: 0.6488 and 0.7457; $2\theta_{max}$ = 61.036°; 87,657 reflections measured, 12,391 unique; R_{int} = 0.0244; number of data/restraint/parameters 12,391/1/494; R_1 = 0.0308 [12,333 reflections, $I > 2\sigma(I)$], $wR(F^2)$ = 0.0797 (all data); largest difference peak 1.437 e Å^{-3}, Flack parameter: −0.0150 (11).

Structural Data for ***6***. $C_{41}H_{58}F_6IrN_4Sb$; M_r = 1034.86; yellow plate, 0.030 × 0.057 × 0.100 mm^3; orthorhombic $Pna2_1$; a = 30.0025 (7) Å, b = 10.5149 (3) Å, c = 13.4963 (3) Å; V = 4257.72 (18) Å^3, Z = 4, D_c = 1.614 g/cm^3; μ = 3.816 cm^{-1}; min. and max. absorption correction factors: 0.6546 and 0.7457; $2\theta_{max}$ = 56.58°; 58,452 reflections measured, 10,432 unique; R_{int} = 0.0413; number of data/restraint/parameters 10,432/2/498; R_1 = 0.0340 [9825 reflections, $I > 2\sigma(I)$], $wR(F^2)$ = 0.0813 (all data); largest difference peak 5.195 e Å^{-3}, Flack parameter: 0.032 (7).

■ ASSOCIATED CONTENT

Supporting Information

The Supporting Information is available free of charge at https://pubs.acs.org/doi/10.1021/acs.organomet.2c00172.

^{1}H and $^{13}C\{^1H\}$ spectra and crystal structure data for the complexes **1**−**4** and **6** (PDF)

Accession Codes

CCDC 2164260−2164264 contain the supplementary crystallographic data for this paper. These data can be obtained free of charge via www.ccdc.cam.ac.uk/data_request/cif, or by emailing data_request@ccdc.cam.ac.uk, or by contacting The Cambridge Crystallographic Data Centre, 12 Union Road, Cambridge CB2 1EZ, UK; fax: +44 1223 336033.

■ AUTHOR INFORMATION

Corresponding Authors

Joaquina Ferrer − *Departamento de Catálisis y Procesos Catalíticos, Instituto de Síntesis Química y Catálisis Homogénea (ISQCH), CSIC—Universidad de Zaragoza, 50009 Zaragoza, Spain*; Email: jfecer@unizar.es

Daniel Carmona − *Departamento de Catálisis y Procesos Catalíticos, Instituto de Síntesis Química y Catálisis Homogénea (ISQCH), CSIC—Universidad de Zaragoza, 50009 Zaragoza, Spain*; orcid.org/0000-0003-4196-5856; Email: dcarmona@unizar.es

Authors

Carlos Ferrer − *Departamento de Catálisis y Procesos Catalíticos, Instituto de Síntesis Química y Catálisis Homogénea (ISQCH), CSIC—Universidad de Zaragoza, 50009 Zaragoza, Spain*

Vincenzo Passarelli − *Departamento de Catálisis y Procesos Catalíticos, Instituto de Síntesis Química y Catálisis Homogénea (ISQCH), CSIC—Universidad de Zaragoza, 50009 Zaragoza, Spain*; orcid.org/0000-0002-1735-6439

Fernando J. Lahoz − *Departamento de Catálisis y Procesos Catalíticos, Instituto de Síntesis Química y Catálisis Homogénea (ISQCH), CSIC—Universidad de Zaragoza, 50009 Zaragoza, Spain*; orcid.org/0000-0001-8054-2237

Pilar García-Orduña − *Departamento de Catálisis y Procesos Catalíticos, Instituto de Síntesis Química y Catálisis Homogénea (ISQCH), CSIC—Universidad de Zaragoza, 50009 Zaragoza, Spain*

Complete contact information is available at: https://pubs.acs.org/10.1021/acs.organomet.2c00172

Notes

The authors declare no competing financial interest.

■ ACKNOWLEDGMENTS

We thank the Ministerio de Economía y Competitividad of Spain (Project PGC2018-095561-BI00) and Gobierno de Aragón (Grupo Consolidado: Catalizadores Organometálicos Enantioselectivos) for financial support. C.F. acknowledges Ministerio de Ciencia e Innovación for a grant.

■ REFERENCES

(1) Welch, G. C.; Juan, R. R. S.; Masuda, J. D.; Stephan, D. W. Reversible, Metal-Free Hydrogen Activation. *Science* **2006**, *314*, 1124−1126.

(2) McCahill, S. J. J.; Welch, G. C.; Stephan, D. W. Reactivity of "Frustrated Lewis Pairs:" Three-Component Reactions of Phosphines, a Borane, and Olefins. *Angew. Chem., Int. Ed.* **2007**, *46*, 4968−4971.

(3) Stephan, D. W.; Erker, G. Frustrated Lewis Pairs: Metal-free Hydrogen Activation and More. *Angew. Chem., Int. Ed.* **2010**, *49*, 46−76.

(4) Stephan, D. W.; Erker, G. Frustrated Lewis Pair Chemistry: Development and Perspectives. *Angew. Chem., Int. Ed.* **2015**, *54*, 6400−6441.

(5) Stephan, D. W. The broadening reach of frustrated Lewis pair chemistry. *Science* **2016**, *354*, No. aaf7229.

(6) Stephan, D. W. Frustrated Lewis Pairs: From Concept to Catalysis. *Acc. Chem. Res.* **2015**, *48*, 306−316.

(7) Scott, D. J.; Fuchter, M. J.; Ashley, A. E. Designing effective "frustrated Lewis pair" hydrogenation catalysts. *Chem. Soc. Rev.* **2017**, *46*, 5689−5700.

(8) Fontaine, F.-G.; Rochette, E. Ambiphilic Molecules: From Organometallic Curiosity to Metal-Free Catalysts. *Acc. Chem. Res.* **2018**, *51*, 454−464.
(9) Paradies, J. From structure to novel reactivity in frustrated Lewis pairs. *Coord. Chem. Rev.* **2019**, *380*, 170−183.
(10) Lam, J.; Szkop, K. M.; Mosaferi, E.; Stephan, D. W. FLP catalysis: main group hydrogenations of organic unsaturated substrates. *Chem. Soc. Rev.* **2019**, *48*, 3592−3612.
(11) Chapman, A. M.; Haddow, M. F.; Wass, D. F. Frustrated Lewis Pairs beyond the Main Group: Synthesis, Reactivity, and Small Molecule Activation with Cationic Zirconocene-Phosphinoaryloxide Complexes. *J. Am. Chem. Soc.* **2011**, *133*, 18463−18478.
(12) Flynn, S. R.; Wass, D. F. Transition Metal Frustrated Lewis Pairs. *ACS Catal.* **2013**, *3*, 2574−2581.
(13) Arndt, S.; Rudolph, M.; Hashmi, A. S. K. Gold-based frustrated Lewis acid/base pairs (FLPs). *Gold Bull.* **2017**, *50*, 267−282.
(14) Bullock, R. M.; Chambers, G. M. Frustration across the periodic table: heterolytic cleavage of dihydrogen by metal complexes. *Philos. Trans. R. Soc., A* **2017**, *375*, No. 20170002.
(15) Khusnutdinova, J. R.; Milstein, D. Metal-Ligand Cooperation. *Angew. Chem., Int. Ed.* **2015**, *54*, 12236−12273.
(16) Johnstone, T. C.; Wee, G. N. J. H.; Stephan, D. W. Accessing Frustrated Lewis Pair Chemistry from a Spectroscopically Stable and Classical Lewis Acid-Base Adduct. *Angew. Chem., Int. Ed.* **2018**, *57*, 5881−5884.
(17) Roters, S.; Appelt, C.; Westenberg, H.; Hepp, A.; Slootweg, J. C.; Lammertsma, K.; Uhl, W. Dimeric aluminum−phosphorus compounds as masked frustrated Lewis pairs for small molecule activation. *Dalton Trans.* **2012**, *41*, 9033−9045.
(18) Boudjelel, M.; Sosa Carrizo, E. D.; Mallet-Ladeira, S.; Massou, S.; Miqueu, K.; Bouhadir, G.; Bourissou, D. Catalytic Dehydrogenation of (Di)Amine-Boranes with a Geometrically Constrained Phosphine-Borane Lewis Pair. *ACS Catal.* **2018**, *8*, 4459−4464.
(19) Carmona, M.; Ferrer, J.; Rodríguez, R.; Passarelli, V.; Lahoz, F. J.; García-Orduña, P.; Cañadillas-Delgado, L.; Carmona, D. Reversible Activation of Water by an Air and Moisture Stable Frustrated Rhodium Nitrogen Lewis Pair. *Chem. − Eur. J.* **2019**, *25*, 13665−13670.
(20) Parker, A.; Lamata, P.; Viguri, F.; Rodríguez, R.; López, J. A.; Lahoz, F. J.; García-Orduña, P.; Carmona, D. Half-sandwich complexes of osmium containing guanidine-derived ligands. *Dalton Trans.* **2020**, *49*, 13601−13617.
(21) Wilkinson, E.-T.; Viguri, F.; Rodríguez, R.; López, J. A.; García-Orduña, P.; Lahoz, F. J.; Lamata, P.; Carmona, D. Strained Ruthenium Complexes Bearing Tridentate Guanidine-Derived Ligands. *Helv. Chim. Acta* **2021**, *104*, No. e2100044.
(22) Alonso-Moreno, C.; Antiñolo, A.; Carrillo-Hermosilla, F.; Otero, A. Guanidines: From Classical Approaches to Efficient Catalytic Syntheses. *Chem. Soc. Rev.* **2014**, *43*, 3406−3425.
(23) White, C.; Yates, A.; Maitlis, P. M.; Heinekey, M. (η^5-Pentamethylcyclo pentadienyl)Rhodium and -Iridium Compounds. *Inorg. Synth.* **1992**, *29*, 228−234.
(24) Cahn, R. S.; Ingold, C.; Prelog, V. Specification of Molecular Chirality. *Angew. Chem., Int. Ed. Engl.* **1966**, *5*, 385−415.
(25) Prelog, V.; Helmchen, G. Basic Principles of the CIP-System and Proposals for a Revision. *Angew. Chem., Int. Ed. Engl.* **1982**, *21*, 567−583.
(26) Lecomte, C.; Dusausoy, Y.; Protas, J.; Tirouflet, J.; Dormond, A. Structure crystalline et configuration relative d'un complexe du titanocene presentant une chiralite plane et une chiralite centree sur l'atome de titane. *J. Organomet. Chem.* **1974**, *73*, 67−76.
(27) Pyykkö, P.; Atsumi, M. Molecular Double-Bond Covalent Radii for Elements Li−E112. *Chem. − Eur. J.* **2009**, *15*, 12770−12779.
(28) Kang, J. W.; Maitlis, P. M. (Pentamethylcyclopentadienyl) rhodium and −iridium complexes. V. Complexes with oxy-ligands and the exchange of methyl protons by deuterium under basic conditions. *J. Organomet. Chem.* **1971**, *30*, 127−133.
(29) Ciancaleoni, G.; Bolaño, S.; Bravo, J.; Peruzzini, M.; Gonsalvi, L.; Macchioni, A. Counterion-dependent deuteration of pentamethylcyclopentadiene in water-soluble cationic Rh(III) complexes assisted by PTA. *Dalton Trans.* **2010**, *39*, 3366−3368.
(30) Banerjee, S.; Soldevila-Barreda, J. J.; Wolny, J. A.; Wootton, C. A.; Habtemariam, A.; Romero-Canelón, I.; Chen, F.; Clarkson, G. J.; Prokes, I.; Song, L.; Peter, B.; O'Connor, P. B.; Schünemann, V.; Sadler, P. J. New activation mechanism for half-sandwich organometallic anticancer complexes. *Chem. Sci.* **2018**, *9*, 3177−3185.
(31) SAINT+, version 6.01: Area-Detector Integration Software; Bruker AXS: Madison, 2001.
(32) SADABS, *Area Detector Absorption Program*; Bruker AXS, Madison, WI, 1996.
(33) Krause, L.; Herbst-Irmer, R.; Sheldrick, G. M.; Stalke, D. Comparison of silver and molybdenum microfocus X-ray sources for single-crystal structure determination. *J. Appl. Crystallogr.* **2015**, *48*, 3−10.
(34) Sheldrick, G. M. A short history of SHELX. *Acta Crystallogr., Sect. A: Found. Crystallogr.* **2008**, *64*, 112−122.
(35) Sheldrick, G. M. Crystal structure refinement with SHELXL. *Acta Crystallogr., Sect. A: Found. Adv.* **2015**, *71*, 3−8.
(36) Farrugia, L. J. WinGX and ORTEP for Windows: an update. *J. Appl. Crystallogr.* **2012**, *45*, 849−854.
(37) Spek, A. L. PLATON SQUEEZE: a tool for the calculation of the disordered solvent contribution to the calculated structure factors. *Acta Crystallogr., Sect. C: Struct. Chem.* **2015**, *71*, 9−18.

https://doi.org/10.1021/acs.organomet.2c00172
Organometallics 2022, 41, 1445−1453